Ultrafast, cross-correlated harmonic imaging through scattering media

Amos Kuditcher, Brian G. Hoover, Markus P. Hehlen, Emmett N. Leith, Stephen C. Rand, and Marian P. Shih

A simple upconversion scheme utilizing 40-fs pulses is shown to permit high-contrast imaging of objects obscured by a highly scattering medium when no ballistic component is evident in the scattered light and imaging is performed with any portion of the scattered light pulse. We present a time-gated, inherently low-pass spatially filtered imaging method that minimizes signal-averaging requirements and greatly facilitates imaging under severe scattering (turbid) conditions. © 2001 Optical Society of America

OCIS codes: 320.7110, 320.2250, 290.7050, 070.0070.

1. Introduction

There is a great need for simple techniques that permit imaging through tissue and other highly scattering media with light as alternatives to the use of damaging ionizing radiation or the use of expensive computational techniques that are heavily reliant on high-speed data processing, such as magnetic resonance imaging. Visible and infrared light of course scatter more than x rays in most materials, but many imaginative ways of extracting image information from the small amount of light transmitted through nearly opaque scattering media have been devised in recent years. A significant limitation to existing optical technologies for such imaging, however, is the contrast limitation that is due to the presence in the detector region of scattered light at the same frequency as the incident beams, but with scrambled wave-vector content. This problem is common to all the time-gated imaging techniques, such as those based on time-domain holography,[1–3] optical coherence tomography,[4] four-wave mixing,[5] Raman scattering,[6] Kerr shutters,[7] and parametric conversion,[8] as well as to approaches suitable for use with continuous-wave sources,[9,10] and it is the chief limitation to speed and contrast in most, if not all, of them. For example, in holographic time-gating, nonimage-bearing light contributes an intense background in the detection plane which reduces the attainable contrast. A harmonic confocal technique has been described in which this problem is greatly alleviated when the image-bearing signal is shifted to a frequency different from that of the background.[8] However, to date this approach has succeeded in imaging only one point at a time in the weak scattering or ballistic limit, rendering practical real-time imagery difficult.

We have extended the harmonic approach by introducing parallelism into the imaging process, eliminating the need for scanning (without incurring a penalty in data processing), and using extremely short pulses to show that imaging is effective even when scattering is so severe that undeviated forward-scattered light (the ballistic component) disappears. In the present research we made use of an enlarged, collimated beam at the fundamental frequency to illuminate the entire object obscured behind the scattering medium. Signal light is generated at the sum frequency of a reference beam and the scattered (object) beam by parametric upconversion in a noncollinear, cross-correlation geometry that permits us to capture entire images at once. The image-bearing signal is separated from the scattered fundamental light by a simple spatial stop, thereby eliminating most of the undesired background intensity.

When this research was performed, A. Kuditcher, B. G. Hoover, M. P. Hehlen, E. N. Leith, and S. C. Rand were with the Department of Electrical Engineering, University of Michigan, Ann Arbor, Michigan 48109-2122. A. Kuditcher is now with Celeste Optics, Incorporated, P.O. Box 1779, Allen, Texas 75002-2518. His e-mail address is akuditcher@celesteoptics.com. M. P. Hehlen is now with the Gemfire Corporation, 2471 E. Bayshore Road, Palo Alto, California 94303. M. P. Shih is with the Department of Physics, Saginaw Valley State University, University Center, Michigan 48710-0001.

Received 24 August 2000.
0003-6935/01/010045-07$15.00/0

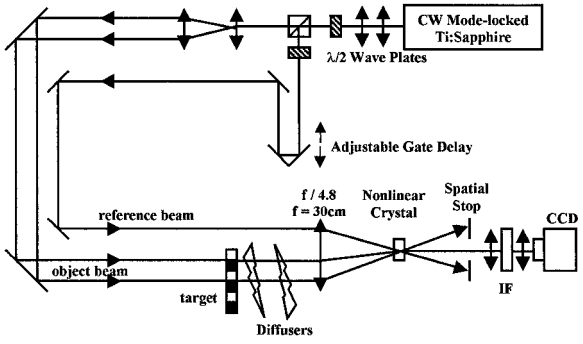

Fig. 1. Apparatus for imaging through highly scattering media with time-gated, sum-frequency generation in a noncollinear, cross-correlation geometry. Double-headed arrows indicate lenses; IF, interference filter; CCD, charge-coupled device camera.

2. Experiment

As indicated schematically in Fig. 1, the output of a Ti:sapphire laser oscillator,[11] emitting cw mode-locked pulses at 798 nm, was expanded by a factor of 2, collimated, and sent through a rotatable half-wave plate to a polarizing beam splitter. This permitted adjustment of the relative intensities in the two optical arms by rotation of the half-wave plate. A second, fixed half-wave plate restored the polarization in the reference arm to horizontal, making it parallel to that of the object beam. The total average power at a pulse repetition rate of 75 MHz was typically 500 mW, and the average power in each arm was generally close to 250 mW for the imaging experiments. We magnified the object beam 5× using a Newtonian telescope, and once again it was collimated. A mechanical translation stage permitted the sampling time gate delay to be adjusted over a range of nearly 10 ps with respect to perfect synchronization of the two pulse trains incident on the cross-correlation crystal.

Magnification of the object beam permitted targets up to 1 cm in diameter to be illuminated from behind. The target that we used to test the imaging capability of the system was an acetate transparency sheet on which a binary rectangular grid pattern of 1-mm spacing was printed. Two pieces of etched antiglare glass, each with a spatial-frequency bandwidth of 300 lines/mm and no specular component, were used in tandem as the diffuser system. These two diffusers were placed immediately downstream of the target. The spacing between the diffusers was gradually increased to 25 cm, at which point the distortion by the diffusers completely obscured the grid pattern from view by conventional photographic imaging. An $f/4.8$ collection lens with a focal length of 30 cm was placed 1 focal length beyond the exit plane of the scattering system. Because the exiting surface of the diffuser was situated at the front focal plane of the collecting lens, there is a two-dimensional Fourier-transform relationship between the light distribution emerging from the target and diffuser arrangement and the light at the back focal plane of the collecting lens. Thus the light distribution at the back focal plane of the collection lens is the transform of the light emerging from the diffuser, or its the spatial-frequency spectrum.

The nonlinear crystal ($LiIO_3$) was placed at the back focal plane of the collecting lens, where the reference beam came to a focus and sampled the Fourier transform of the scattered light distribution there. In this configuration of the cross correlator (Fig. 1), the function of the nonlinear crystal is twofold: (1) it acts as a coincidence gate that shutters whatever object beam light arrives simultaneously with the reference beam, and (2) it acts as a low-pass spatial filter. The latter is due to the phase-matching constraints of the crystal.

An oriented crystal of $LiIO_3$ was used for cross correlation. $LiIO_3$ has a smaller acceptance angle for parametric upconversion than many other nonlinear crystals, which is disadvantageous for most nonlinear applications. However, as discussed in Section 4, reduction of the acceptance angle actually improves the capability with the present technique to perform imagery with light from the trailing edge of the scattered wave. Other design considerations took into account the performance characteristics of the $LiIO_3$ nonlinear crystal, which are well known.[12] For example, this material has a very high nonlinear coefficient ($d_{31} = -4.4$ pm/V) and exceptionally low loss for near-infrared light.[12,13] The crystal was cut and polished for angle-tuned, second-harmonic generation at a wavelength of 800 nm, in accordance with (1) the index of refraction for the ordinary ray $n_o = 1.8676$ at 800 nm, (2) the index of refraction for the extraordinary ray $n_e = 1.7245$ at 800 nm, (3) and their respective dispersion (Sellmeier) equations[12]:

$$n_0^2(\lambda) = 3.4132 + 0.0476/(\lambda^2 - 0.0338) - 0.0077*\lambda^2,$$

$$n_e^2(\lambda) = 2.9211 + 0.0346/(\lambda^2 - 0.0320) - 0.0042*\lambda^2.$$

Because the crystal has a nominal dispersion of $n_o'' = 9.48$ fs^2/mm for ordinary rays, the crystal thickness was limited to 1 mm to avoid excessive pulse broadening. As shown in Fig. 2, the fit of a sech^2 distribution to the autocorrelation trace, measured with no scattering medium present, yielded a pulse width of $\tau_p = 38$ fs.

The crossing angle of the light beams in the crystal was 4 deg, as large a value as possible given the dimensions of our focusing lens. This provided adequate spatial separation of the signal beam from both inputs, although it was not large enough to prevent detectable doubling of the individual beams. When the phase-matching angle of the nonlinear crystal was adjusted for cross-correlation and the object pulse and reference pulse arrivals were synchronized with the delay line, a faint sum-frequency signal emerged in the forward direction and was isolated. A spatial stop blocked the object and reference beams on either side, while at the same time allowing the signal to pass. Light at the fundamental wavelength (800 nm) was subsequently blocked with a 10-nm bandwidth interference filter centered

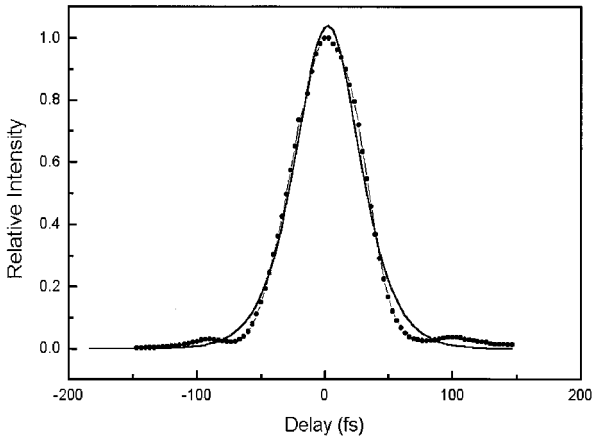

Fig. 2. Signal-averaged, second-harmonic generation cross-correlation trace (dotted curve) of the incident pulses in the absence of any diffuser together with the least-squares fit to a sech^2 pulse shape (solid curve).

at 400 nm, and the signal was imaged onto a CCD camera, as indicated in Fig. 1.

From a signal recording standpoint, the relative insensitivity of the detector to the operating wavelength presented the most severe limitation to the image recording process. The wavelength of the parametrically upconverted signal (400 nm) to be recorded was substantially shorter than the wavelength for peak sensitivity (650 nm) of the CCD, resulting in loss of sensitivity by a factor of ~50. The 16-bit CCD camera was a Model EEV576 manufactured by Princeton Instruments with an active area consisting of 576 × 384 pixels, each 23.5 μm on a side. The maximum readout rate was 100 kHz, limiting complete array readout time to 2.2 s/frame.

A second major limitation in our setup was self-doubling in the nonlinear crystal, in which individual input beams undergo second-harmonic generation and produce ultraviolet output comparable to the upconverted, cross-correlation signal. Some of this light can scatter from imperfections in the nonlinear crystal to enter the detector. Noise from this mechanism was reduced by an appropriate choice of a lens with both a large diameter [3 in. (8 cm)] and a small f-number ($f/4.8$) to create the largest angle possible at the Fourier plane and to maximize the separation between the beams. Without the careful elimination of even the weakest extraneous scattering surfaces in the optical system, the level of scatter background noise would have made imagery of the signal impossible.

The angular scattering characteristics of the diffuser were determined by a simple secondary experiment described in Fig. 3. A collimated laser beam illuminated the diffuser(s) from behind, and the light emerging from the diffuser(s) was collected by a lens. A CCD camera, placed at the back focal plane of the lens, recorded the magnitude of the two-dimensional Fourier transform of the diffuser. The image on the CCD camera is the spatial-frequency spectrum of the diffuser and quantitatively displays its scattering

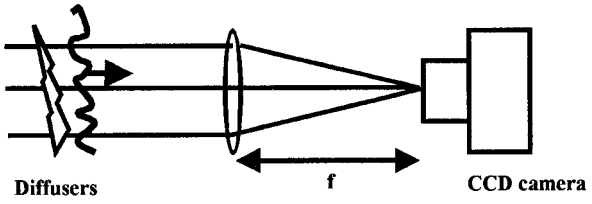

Fig. 3. Apparatus used to verify that the forward-scattering diffuser contains no ballistic component.

properties of the diffuser. Examination of the Fourier distribution is an exacting test for the presence of light that has undergone little or no scattering (i.e., a ballistic component).

Figure 4(a) is the intensity distribution of the object beam at the Fourier-transform plane, in the absence of diffusers. The bright dot at the center demonstrates that the spatial-frequency content of the undistorted light is predominantly dc, or forward moving. A line scan of the intensity distribution

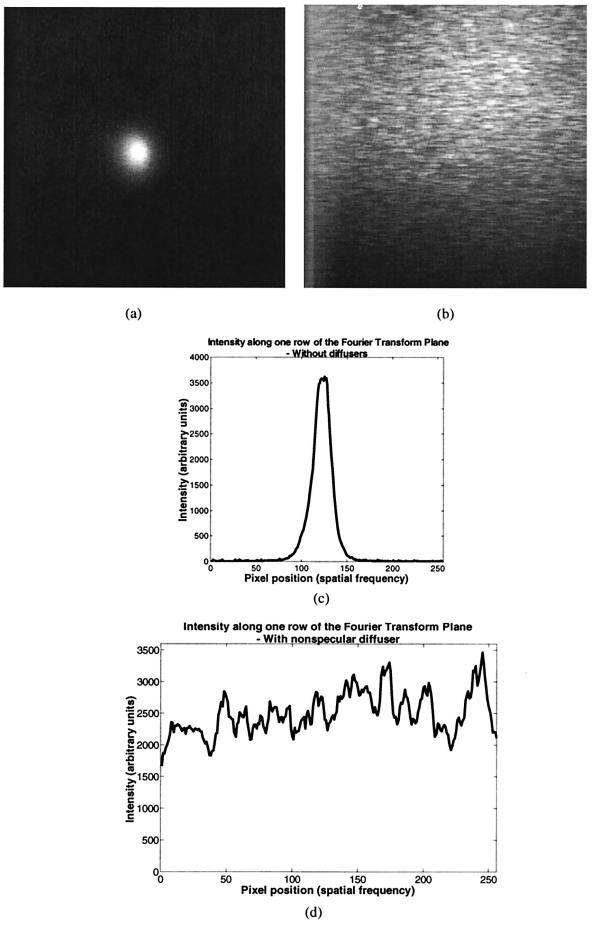

Fig. 4. Image of the Fourier-transform plane (a) with no diffuser present, (b) with the diffuser system in place. In the central part of (b) that corresponds to spatial frequencies near dc, note the absence of any narrow forward-scattering peak, indicating the absence of the ballistic component. This distribution is broadly peaked in the forward direction. Disregard its slight off-axis displacement, which is due to a wedge in the diffuser system. (c) and (d) Intensity plots of (a) and (b), respectively, for one row of pixels.

along one row of pixels [Fig. 4(c)] reveals the sharply peaked distribution of spatial frequencies directly. When a diffuser with a specular (or ballistic) component is placed in the optical system in Fig. 3, its Fourier-transform plane (not shown) would reveal a bright, central specular component superimposed on a uniform halo of higher spatial frequencies of scattered light.

More strongly scattering diffusers with no specular component at all show only a smooth, broad distribution of spatial frequencies. Figure 4(b) shows that the diffuser, used for imaging in the present research, has no specular (or ballistic) component. The bright spot signaling the presence of ballistic light is not present. Instead, only a uniform smear of low-contrast speckle is visible. The intensity plot, Fig. 4(d), of one row of pixels of this pattern bears this out. The data in Figs. 4(b) and 4(d) clearly indicate that no central peak with the angular spread of the ballistic light was present in the scattered light distribution. Hence the imaging results reported in Section 3 were obtained under much more severe scattering conditions than in previous experiments where the presence of a ballistic component permitted temporal gating alone to select the best image-bearing component of the scattered light.[7]

Our method is effective for both diffusers with an observable ballistic (i.e., specular) component and diffusers without. When a ballistic component is present, the reference beam can be synchronized with the ballistic light which yields a sharp high-resolution image, without data processing, as quickly as the array can be read out. In this case, our approach extends previous ultrafast time-gated imaging techniques[1–10] only by introducing parallelism and inherently high contrast. Yet remarkably, as we show in Section 3, with a combination of temporal gating and spatial filtering, imaging can still be performed successfully when no ballistic component is present as well.

The experimental results reported in this paper are for images formed through diffusers that have no specular component. For such severe scatterers, the abundance of forward-traveling light disappears, and the utility of time gating as an ultrafast shutter rapidly diminishes when applied in isolation. Then light emerging from the scattering medium generally contains enough randomized wave-vector bandwidth per unit time that image information is highly distorted at all delays. Nevertheless, as shown experimentally here, and as we explain in Sections 3 and 4, use of very short pulses in combination with phase-matched frequency conversion techniques can facilitate effective imaging in this regime. Signals from time slices anywhere within the scattered object pulse provide satisfactory imaging when angular selectivity is combined with time gating in the detection scheme. Even at the low average power levels attainable from cw mode-locked oscillators, this method is successful without electronic processing of the image.

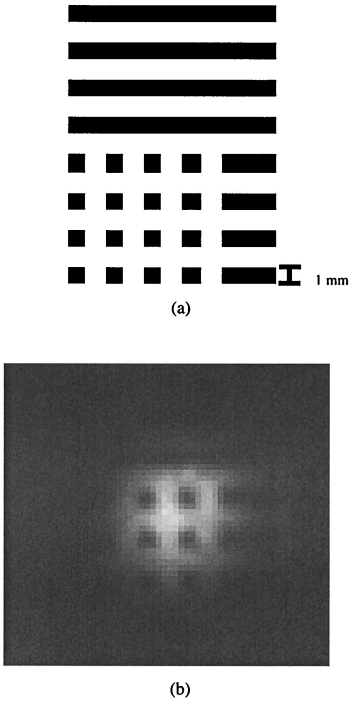

Fig. 5. (a) Resolution target, consisting of 1-mm squares and lines, to be imaged. The diffuser completely obscures this target. (b) Image recorded with the sum-frequency optical system in Fig. 1. (The uncorrelated background field was subtracted out.)

3. Results

In Fig. 5(a) the rectangular grid pattern fabricated for use as a resolution target is reproduced. This is, in fact, what a photograph of the target would look like in the absence of the diffuser system. The separation and thickness of all lines on the target are 1 mm. When hidden behind the two nonspecular diffusers, as described in Section 2, the target is completely invisible to conventional photographic recording and simply yields a uniform, featureless speckle pattern. Thus, without the benefit of our technique, the target was entirely hidden by the diffusers, and its photograph therefore is not included in this paper. The principal result of the ultrafast cross-correlated harmonic imaging technique is shown in Fig. 5(b) where the 1-mm grid is visible. The good fidelity of its details demonstrates that our technique has overcome the severe scattering conditions that were imposed by our choice of diffuser. This demonstrates that our approach to imaging works and that imaging through severe diffusers is possible.

Features as small as 1 mm are well resolved by this technique. In practice it was found that imaging target features that are smaller than those of this grid pattern resulted in degraded imagery. The spatial resolution in our experiment was limited by the finite pulse width of our timing gate. Light from two points situated a distance d apart at the exit surface of the first diffuser can combine, scatter in the same direction, and pass through the gate together if $d < (CD\tau_p)^{1/2} \sim 1.68$ mm. A second factor that potentially

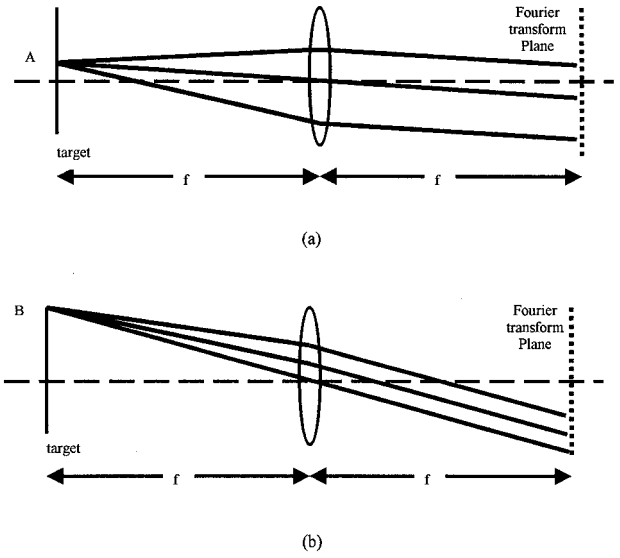

Fig. 6. Diagram tracing rays of the vignetting of the image in Fig. 5(b). (a) If the shallow parallel rays satisfy the phase-matching condition of the nonlinear crystal, then (b) steeper parallel rays, originating from a more extreme point on the object, will not.

limits spatial resolution and causes vignetting of the image is the spot size of the reference beam, considered later in this paper. The only image processing used in preparing Fig. 5(b) for publication was a simple subtraction of a recording of the static scattered-field pattern, which was due to the imperfections of the nonlinear crystal at the harmonic frequency made with the delay line adjusted to maximum delay. Images degraded by scattering from defects in the nonlinear crystal can easily be removed in this manner.

Examination of Fig. 5(b) reveals that the radial extent of the image is somewhat limited. The center circular portion of the target grid is visible, but the outer surroundings are entirely black. This vignetting effect is due to the limited acceptance angle $\Delta\theta$ of the angle-tuned nonlinear crystal. Consider, as shown in Fig. 6, the target and the diffusers at the front focal plane of the collecting lens. Rays originating from a portion of the target (A) that is near the optical axis will emerge from the lens with a lower spatial frequency, as indicated by the shallow parallel rays in Fig. 6(a). Rays originating from a portion of the target that is farther from the optical axis will emerge from the lens with a higher spatial frequency, as indicated by the steeper parallel rays in Fig. 6(b). Because the nonlinear crystal is located at the Fourier-transform plane of this lens, the reference beam overlaps a limited range of spatial coordinates where upconversion can take place. This results in spatial filtering of the distribution of field amplitudes and phases in the transform plane. Rays from point A in the target that fall within the reference beam area can undergo upconversion and contribute their phase and amplitude to image formation by the coherent cross-correlation process, provided that in addition their directions fall within the acceptance angle of the nonlinear crystal. However, rays from B that fall outside the reference beam area will not contribute to the image.

We can analyze this qualitative explanation of the vignetting in Fig. 5(b) by representing the target $u(x)$ in polar form, namely, $u(x) = a(x)\exp[i\phi(x)]$. The field arriving at the Fourier-transform plane of the collecting lens is

$$U(f_x) \equiv \mathcal{F}[u(x)] = \mathcal{F}[a(x)] * \mathcal{F}\{\exp[i\phi(x)]\}, \quad (1)$$

where $*$ is the convolution operator. Passage through the reference beam spot, located at the Fourier-transform plane, is equivalent to propagation through a low-pass spatial-frequency filter, described as a multiplication by $\mathrm{rect}(f_x/\Delta f_s)$. The filtered transform is thus

$$U(f_x)\mathrm{rect}(f_x/\Delta f_s) = \mathcal{F}[a(x)] * \mathcal{F}\{\exp[i\phi(x)]\}\mathrm{rect}(f_x/\Delta f_s), \quad (2)$$

and the final image is the inverse Fourier transform:

$$\begin{aligned}\mathcal{F}^{-1}[U(f_x)\mathrm{rect}(f_x/\Delta f_s)] &= \mathcal{F}^{-1}(\mathcal{F}[a(x)] * \mathcal{F}\{\exp[i\phi(x)]\} \\ &\quad \times \mathrm{rect}(f_x/\Delta f_s)) \\ &= u(x) * \mathrm{sinc}[(\Delta f_s)(x)]. \quad (3)\end{aligned}$$

The final image is the original target, modulated by a sinc function. The width of the sinc function, which is twice the distance from the zeroth-order maximum to the first null, is $2\Delta f_s$. When the nonlinear crystal is configured at the Fourier-transform plane, the spatial frequency bandwidth that will upconvert is $\Delta f_s = \Delta\theta/\lambda_0$. The acceptance angle for $LiIO_3$ is 19×10^{-3} deg.[12] At 800 nm, the predicted width of the field of view is 4.8 mm, which agrees with the size of the circular portion of the target that can be seen in our results in Fig. 5(b).

The tolerance with which the delay line had to synchronize the reference pulse with the object beam pulse depended on the presence or absence of a ballistic component. For diffusers possessing a specular component, it was necessary to adjust the relative timing of the reference and object beams to within one pulse width to obtain the optimum signal. This is not surprising, because the undistorted input beams must overlap both temporally and spatially within the nonlinear crystal to generate a signal wave. Correspondingly, because the beams were arranged to cross at an angle, displacement of the nonlinear crystal by a distance less than its thickness (1 mm) resulted in the complete disappearance of the cross-correlation signal when there were no diffusers present.

In the presence of diffusers with no specular component, the nonlinear crystal could be moved along the optical axis over the full range of the translation stage (at a fixed pulse delay) without any apparent change in signal intensity. We discovered that clarity and brightness of the image was maintained as the crystal was translated by 1.0 cm along the cross-correlation axis. This observation was a key result

of the present research and demonstrated two things. First, because cross correlation occurred at positions separated by 1 cm, the reference beam necessarily intercepted off-axis portions of the scattered wave front within the thin $LiIO_3$ crystal that were delayed by more than 30 ps. Pulse stretching was thereby confirmed to be substantial under the experimental conditions depicted in Fig. 4(b), amounting to at least this time interval. Second, the fact that images were observed over a range of positions of the nonlinear crystal clearly indicated that, with the detection technique used here, late-arriving light can be just as useful for image formation as early-arriving light, provided that an appropriate combination of selective procedures is used for detection.

The data for the image in Fig. 5(b) were acquired in an accumulation time of 20 s. This acquisition time corresponded to that needed to saturate the most brightly illuminated pixel at the power levels used in the experiment. At equivalent power levels, good but less intense images (only 1000 counts in the brightest pixel) could be obtained in approximately 40 ms. At higher input powers, the recording time for unsaturated images was correspondingly reduced. In view of this it is clear that, with this approach, dynamic imagery with frame times of less than 40 ms can be readily achieved with available oscillator powers without resorting to data processing of any kind.

4. Discussion

Temporal gating is known to be ineffective on its own in forming images of objects obscured by scattering media when late-arriving light is used. This is because late-arriving light consists of many sets of scattered rays that follow different vectorial routes in three dimensions through the medium. However, as our results show, and as we discuss below, use of vectorial constraints can overcome this problem by providing the additional selectivity necessary to isolate individual trajectories.

Our results show that ultrafast harmonic imaging works well under nonspecular scattering conditions, when no ballistic component is evident in light transmitted by the medium. Also, late-arriving light can produce good images. Hence when time gating is used at any point within a stretched, scattered image pulse in combination with directionally selective (vectorial) detection, we have shown that high-quality images can be formed. Sets of rays that follow similar, but not identical, vectorial routes through the medium develop only a small spread in constant relative phase. Such rays are capable not only of forming images, but of generating phase-matched parametric output. The upconverted image quality therefore depends on the degree to which the spread in phases can be restricted in the detection process, regardless of how complex their trajectories may be or what total temporal delay the ray trajectory incurs. In previous time-gated imaging experiments, the detection methods did not to our knowledge incorporate the vectorial selectivity necessary to demonstrate the results shown here.

A combination of fast temporal gating and angularly selective detection is functionally equivalent to gated off-axis, confocal spatial filtering with a vanishingly small pinhole. Such a spatial-filtering transformation results in perfect imaging in the strong scattering limit.[10] Ultrashort time gating by itself minimizes the spread in delay times for sampled light, but makes no distinction, for example, between on-axis multiply scattered light and off-axis light with the same delay. Hence time-gated, late-arriving light from a highly scattering medium consists of a superposition of incoherent components unsuitable for imaging. For off-axis light originating from the passage through a small fixed number of scattering vertices, however, a relatively well-defined family of trajectories symmetric about the propagation axis can be defined when we specify both the delay and the projection of the initial (or final) wave vector on the propagation axis. Furthermore, if the family of off-axis trajectories is then restricted to essentially a single path, the phase distribution is narrow enough that high-quality upconversion imaging becomes possible. In this paper we have experimentally implemented detection of this type by efficiently upconverting only time-gated light with wave vectors satisfying a crossed-beam, phase-matching condition. This approach limits the contributing rays to those sharing a common plane of origin (perpendicular to the axis) and an initial scattered wave vector, to an extent determined jointly by the temporal gate width and the crystal acceptance angle. By sampling a restricted set of scattering trajectories, ones not scrambled and distorted by other contributions of altogether different phase, we can achieve high-quality imagery. Spatial resolution is determined by reference beam pulse width and spot size, and the field of view is limited by the acceptance angle of the cross correlator.

The observation in this research that late-arriving portions of the scattered light can be used for imaging immediately raises the question of what limitations there may be in the use of shorter and shorter pulses in combination with more and more angular selectivity in imaging through severe scatterers. For arbitrarily small upconversion acceptance angles and pulse widths, it might be concluded at first that our ability to image through scattering media with a harmonic cross-correlation technique is unlimited. Not surprisingly, this premise is incorrect, as we now discuss.

There are several limitations that can be anticipated. As pulses are shortened, their frequency bandwidth increases. Only a limited bandwidth can contribute to image formation, however, because phase matching in the nonlinear crystal can be achieved only over a limited range, say $\Delta\omega$. Hence use of pulse widths shorter than $\tau = (\Delta\omega)^{-1}$ reduces the signal level without improving temporal resolution. However small the acceptance angle $\Delta\theta$ may be, it is finite, and the range of phase-matchable wave vectors incident on the crystal Δk is therefore limited

by angular dispersion over $\Delta\theta$. This means that pulses shorter than

$$\tau = (c\Delta k)^{-1} = \left[ck_0 \left(\frac{\partial n}{\partial \theta} \right) \Delta\theta \right]^{-1}$$

cannot be entirely phase matched in angle-tuned crystals. Because the angular spread $\Delta\theta$ determines a spatial-frequency bandwidth of $\Delta f = \Delta\theta/\lambda_0$, there is a minimum acceptable gate width

$$\tau = \left[c \left(\frac{\partial n}{\partial \theta} \right) 2\pi\Delta f \right]^{-1}$$

for any desired spatial resolution. This point was recently confirmed in spatial-filtering experiments.[14]

In our optical system configuration (Fig. 1) in which the nonlinear crystal is located at the Fourier-transform plane, one of the two factors limiting the resolution of our imaging process is the area over which upconversion occurs. The bandwidth of what is effectively a low-pass spatial filter is determined by the spot size of the reference beam at the point of cross correlation because only those spatial frequencies that overlap with the reference beam can upconvert into the imaged signal. Thus, for a laser constrained to a fixed amount of power, there is a trade-off between resolution and conversion efficiency. On the other hand, nonlinear crystals of this type are usually not placed at the Fourier-transform plane, and alternative optical systems that differ from Fig. 1 in this manner would face different imaging limitations. For example, the finite size of the nonlinear crystal limits the spatial frequencies contributing to image formation. Even if all scattered light were arranged to impinge on the crystal input face within the acceptance angle, the wave-vector bandwidth would undergo vignetting in the Fourier-transform plane, owing to the crystal aperture.

Finally, as the severity of scattering increases, the average number of scattering events increases. The diversity of scattering paths corresponding to a particular gate time and width therefore increases nonlinearly as the transport mean free path l^*, or the distance a between the scatterers shortens. Under these circumstances, linear changes in gate width or upconversion area (acceptance angle for placement away from the transform plane) should become progressively less effective in selecting unique trajectories from the multitude of scattered rays with sufficient phase definition to achieve phase matching and form high-quality images. In the correlated scattering regime the net phase will cease to be well defined on arbitrarily complex trajectories when either a, the interparticle separation, or l^* become less than λ. In this extreme scattering limit, we can expect image quality to decline beyond our ability to restore it with shorter pulses or better cross-correlator characteristics at predictable values of the transport mean free path, interparticle separation, and sample thickness.

This research was supported in part by the Research Corporation, by U.S. Army Research Office grant DAAH-04-96-0254, and by the U.S. Air Force Office of Scientific Research under grant F49620-98-1-0189. M. P. Hehlen is indebted to the Swiss National Science Foundation for financial support.

References

1. K. G. Spears, J. Serafin, N. H. Abramson, X. Zhu, and H. Bjelkhagen, "Chronocoherent imaging for medicine," IEEE Trans. Biomed. Eng. **36,** 1210–1214 (1989).
2. Y. Chen, Y. Chen, D. Dilworth, E. Leith, J. Lopez, and J. Valdmanis, "Two-dimensional imaging through diffusing media using 150-fs gated electronic holography techniques," Opt. Lett. **16,** 487–489 (1991).
3. E. Leith, C. Chen, H. Chen, Y. Chen, D. Dilworth, J. Lopez, J. Rudd, P.-C. Sun, J. Valdmanis, and G. Vossler, "Imaging through scattering media with holography," J. Opt. Soc. Am. A **9,** 1148–1153 (1992).
4. D. Huang, E. A. Swanson, C. P. Lin, J. S. Schuman, W. G. Stinson, W. Chang, M. R. Hee, T. Flotte, K. Gregory, C. A. Puliafito, and J. G. Fujimoto, "Optical coherence tomography," Science **254,** 1178–1181 (1991); M. R. Hee, J. A. Izzat, J. M. Jacobson, J. G. Fujimoto, and E. A. Swanson, "Femtosecond transillumination optical coherence tomography," Opt. Lett. **18,** 950–952 (1993).
5. M. A. O'Leary, D. A. Boas, B. Chance, and A. G. Yodh, "Experimental images of heterogeneous turbid media by frequency-domain diffusing-photon tomography," Opt. Lett. **20,** 426–428 (1995).
6. J. Reintjes, M. Bashkansky, M. Duncan, R. Mahon, L. L. Tankerskley, J. A. Moon, C. L. Adler, and J. M. S. Prewitt, "Time-gated imaging with nonlinear optical Raman interactions," Opt. Photon. News **4,** 28–32 (1993).
7. L. Wang, P. P. Ho, C. Liu, G. Zhang, and R. R. Alfano, "Ballistic 2-D imaging through scattering walls using an ultrafast optical Kerr gate," Science **253,** 769–771 (1991); L. Wang, P. P. Ho, X. Liang, H. Dai, and R. R. Alfano, "Kerr–Fourier imaging of hidden objects in thick turbid media," Opt. Lett. **18,** 241–243 (1993).
8. K. M. Yoo, Q. Xing, and R. R. Alfano, "Imaging objects hidden in highly scattering media using femtosecond second-harmonic-generation cross-correlation time gating," Opt. Lett. **16,** 1068–1070 (1991).
9. H. Chen, Y. Chen, D. Dilworth, E. Leith, J. Lopez, M. Shih, P.-C. Sun, E. Arons, and K. Clay, "Comparison of various holographic techniques for imaging through biological tissue," in *Holographic Imaging and Materials*, T. H. Jeong, ed., Proc. SPIE **2043,** 272–277 (1993).
10. E. Arons and D. Dilworth, "Analysis of Fourier synthesis holography for imaging through scattering materials," Appl. Opt. **34,** 1841–1847 (1995).
11. C.-P. Huang, H. C. Kapteyn, J. W. McIntosh, and M. M. Murnane, "Generation of transform-limited 32-fs pulses from a self-mode-locked Ti:sapphire laser," Opt. Lett. **17,** 139–141 (1992).
12. V. G. Dmitriev, G. G. Gurzadyan, and D. N. Nikogosyan, *Handbook of Nonlinear Optical Crystals*, 2nd ed., Optical Science Series (Springer-Verlag, Berlin, 1995), Vol. 64, pp. 103–106.
13. Specifications can be obtained at supplier's URL: http://geology.uiggm.nsc.ru/uiggm/monokrys/produkt/iodat_e.htm.
14. E. N. Leith, B. G. Hoover, S. M. Grannell, K. D. Mills, H. S. Chen, and D. S. Dilworth, "Realization of time gating by use of spatial filtering," Appl. Opt. **38,** 1370–1376 (1999).